Hydrothermal Synthesis of W-Doped Titania Nanofibers and Its Photocatalytic Activity

[1]Low Jing Xiang, [*2]Teressa Nathan-Walleser

Faculty of Engineering, Multimedia University
Jalan Multimedia, Cyberjaya 63000 Malaysia

[1] jx_low@yahoo.com; [2*]teressanathan@hotmail.com

Abstract

Titania nanofibers were synthesized using hydrothermal technique by dispersing P25 powder (20% Rutile and 80% Anatase of TiO_2) in NaOH solution and annealed at 150 ^oC. The nanofibers that were in ten-hundred nanometer lengths with the diameter of ~ 10 nm were doped with Tungsten Oxide (WO_3) using a simple and efficient impregnating-calcination method. The doping effect of Tungsten (W) on TiO_2 was investigated by means of XRD, UV-Vis and gas chromatograph, while SEM and Nitrogen adsorption were carried out to investigate the morphology and the Brunauer-Emmett-Teller (BET) surface area respectively. The result showed that W doping has enhanced the visible light photocatalytic activity of TiO_2 nanofibers as it has induced shift in the absorption light range with the narrowing of the bandgap energy. The photocatalytic activity of the W-doped anatase TiO_2 has greatly enhanced the transportation of charge transfer and reduced the electron-hole recombination. It showed more than 60 times higher photocatalytic activity than TiO_2 nanofiber and pristine Degussa P25. The amount of W-doping played a crucial role in affecting the photocatalytic activity of TiO_2 where W-doping of more than 5% can reduce the photocatalytic efficacy under visible light range.

Keywords

Metal Oxides; Nanostructures; Band-structure; Photocatalytic

Introduction

Photocatalyst water splitting hydrogen production has been receiving great attention for its high potential as a source of energy, which can be obtained from solar irradiation and water. With Gibbs energy of 237.7 $kJmol^{-1}$, photocatalyst water splitting is quite a challenging process as it yields thermodynamically unfavorable reaction (Fujishima, 1972; Kudo, 2033; Khan, 2008). However, semiconductor photocatalyst materials overcame this shortfall by band structure tuning, whereby the efficiency of water splitting is determined by the band structure of the material and the electron transfer process. A photogenerated electron is produced in the conduction band along with photogenerated holes in the valence band when the semiconductor photocatalyst material is subjected to irradiation of light energy source (Kaneko, 2002) and this affects the recombination rate. Therefore, band structure tuning has become imperative for the design of semiconductors with these properties.

Years since the discovery of photo-induced water splitting process on TiO_2 electrode by Fujishima and Honda (1972) , TiO_2 has been proven as the most suitable, cost effective and environmental friendly photocatalyst materials for widespread hydrogen production with chemical inertness, non-toxicity, photostability and high oxidizing power properties (Fujishima, 1972; Fujishima, 2000). However, the application of TiO_2 in photocatalysis field is limited by its wide bandgap energy, 3.2 eV and 3.0 eV for Anatase TiO_2 and Rutile TiO_2 respectively, where UV irradiation is needed to activate its photocatalytic properties (Fujishima, 2008). As a result, only 3-5% of the solar beam that reaches the earth can be utilized, which is inefficient. In the past, research efforts have been focused on decreasing the threshold energy for excitation during TiO_2-assisted photocatalysis to maximize the utilization of a wider fraction of solar irradiation for energy conversion as TiO_2 has a relatively large bandgap.

The photocatalytic activity of photocatalyst materials can be improved by several methods such as coupling TiO_2 with other metal oxides, doping, sensitization and supporting (Hashimoto, 2005; Colon, 2006; Kanade, 2007; Arai, 2008). Doping metal ion on the surface of the material has been reported to suppress the electron-hole recombination rate on the photocatalyst materials surface (Colon, 2006; Kanade, 2007; Arai, 2008). The photocatalytic activity was also found to increase with the surface area, which resulted from the doping (Jung, 1999; Dholam, 2009). Transition metal ion has been proven to provide additional energy levels within the bandgap of semiconductor as the metal ion doping creates a

transition band on the photocatalyst materials. This may significantly improve the light absorption range of the photocatalyst materials (Zhou, 2005; Zhou, 2006).

Tungsten (W) is amongst the metal ion that has high potential as a dopant on the photocatalyst materials as it is non-toxic and low in cost (Shen, 2005; Couselo, 2008). Its smaller bandgap energy of 2.8 eV has been reported to improve the electron-hole recombination rate, because it controls the availability of photoexcited sites on the catalyst surface. It was also found to improve the charge separation which resulted from the coupling of the two materials (Putta, 2011). $W^{(6+)}$ in WO_3 acts as a trapping site by accepting photoexcited electrons from TiO_2 valence band and reduces to $W^{(5+)}$. In the present work, W-doping has been used to shift the absorption edge of anatase TiO_2 to the visible region and modify its electronic structure by substituting oxygen in the lattice, with tungsten. W-doped TiO_2 nanofibers were synthesized by a simple single step impregnating-calcination method using Titania nanofiber as precursors. The sample was subjected to physical characterization such as XRD, SEM, nitrogen adsorption and UV-Vis characterization to confirm the structural properties and then evaluated for its photocatalytic hydrogen production in methanol aqueous solution by visible light irradiation.

Experimental

Preparation of TiO_2 Nanofiber

TiO_2 nanofiber was prepared by hydrothermal method using Degussa P25 (composed of 80% Anatase and 20% Rutile) as a starting material. 0.75 g of P25 was added into 70 ml of 10 M NaOH solution and stirred for 20 minutes. Solution was then heated up at 150°C in a 100 ml Teflon-lined autoclave for 48 h to ensure the complete combustion of NaOH and the formation of highly crystalline nanofibers. The resulted precipitation was separated by filtration and washed with 0.1 M HCl solution and distilled water. Sample was then dried at 80°C.

Preparation of W-doped TiO_2 Nanofiber

Impregnation method was used to prepare W-doped TiO_2 nanofiber by mixing 0.2 g of TiO_2 with sodium tungsten dehydrate solution at various loading level such as 1, 2.5, 5 and 10 wt%. Nitrate acid solution was used to adjust the pH value of the solutions to 5 followed by 0.5 h of continuous stirring. Solutions were then left at room temperature for 48 h before being dried it in the oven at 100 °C for 5 h to evaporate the water. Dried samples were then calcined at 550 °C for 1.5 h in a muffle furnace.

Physical Characterization of Titania Nanofiber

X-ray diffraction patterns were obtained using the D/MAX-RB X-Ray diffractometer (Rigaku, Japan) with Cu Kα radiation at a scan rate of 2θ of 0.05 $^{o}s^{-1}$. The accelerating voltage and applied current were at 40 kV and 80 mA, respectively. The absorption and reflectance spectra of sample were recorded using a UV-Vis spectrophotometer (UV-2550, Shidmadzu, Japan). The Brunauer-Emmett-teller (BET) surface area of the sample materials was measured using ASAP 2020 nitrogen adsorption apparatus (Micromeritics Instruments, USA). All samples were subjected to a degassing process at 180°C prior to the nitrogen absorption measurements. The adsorption data in the relative pressure (P/P_0) ranging from 0.05-0.3 were obtained to determine the BET surface area by multi-point BET method. Barret-Joyner-Halender (BJH) method was carried out to determine the pore size distribution of sample materials, assuming that they are all cylindrical pores. Pore volume and average pore size were determined by nitrogen adsorption volume at the relative pressure (P/P_0). Microstructural observation was done using the S-4800 field emission scanning electron microscope (FESEM, Hitachi,Japan).

Photocatalytic Activity Measurements

50 mg of the sample was dissolved in 80 ml of 25% methanol and 75% DI water solution. A 100 ml closely sealed Pyrex flask was used as a reactor at atmospheric pressure and room temperature. The mixture was then poured into the flask and bubbled with nitrogen for 40 minutes to remove dissolved oxygen and ensure that the reaction is under anaerobic conditions. The Pyrex flask with the sample solution was then irradiated by a 350 W Xe arc lamp with 400 nm range with cutoff filter for 1 h. Subsequently, 40 ml of gas was intermittently sampled through septum and analyzed with a gas chromatograph (GC-14C, Shidmadzu, Japan) with nitrogen as the carrier gas.

Results and Discussion

SEM Observation

Fig. 1 (a) and Fig. 1 (b) show the SEM image of undoped TiO_2 nanofiber and W-doped TiO_2 nanofiber, respectively, where monodispersed fibers can be observed whose length ranges from tens to hundreds nanometer, and the diameters were about 10nm. The formation of the nanofibers was initialized by

breaking down the Ti-O-Ti building blocks of the P25 with the aid of NaOH. It was further exfoliated into smaller flakes in the direction of [0 1 0] plane as it was subjected to high pressure and temperature during the hydrothermal process. Both sides of the P25 flakes brimmed with unsaturated dangling bonds which resulted from the high surface activity of P25 flakes. The saturation of these dangling bonds led to different surface energy, hence, further rolling the sheets into fibers (Kasuga, 1998). The adhesion of the layer was determined by the weak van der Waal's forces which caused the hydrophilic head of P25 to bond strongly to the adjacent water molecules (Kasuga, 1998). Fig. 1 (b) shows that when 5% W is doped into TiO_2 nanofiber, the TiO_2 nanofibers tend to agglomerate some sub-particles which are also in the order of nanometer. This may be attributed to the calcination process which has improved the surface activity of sample.

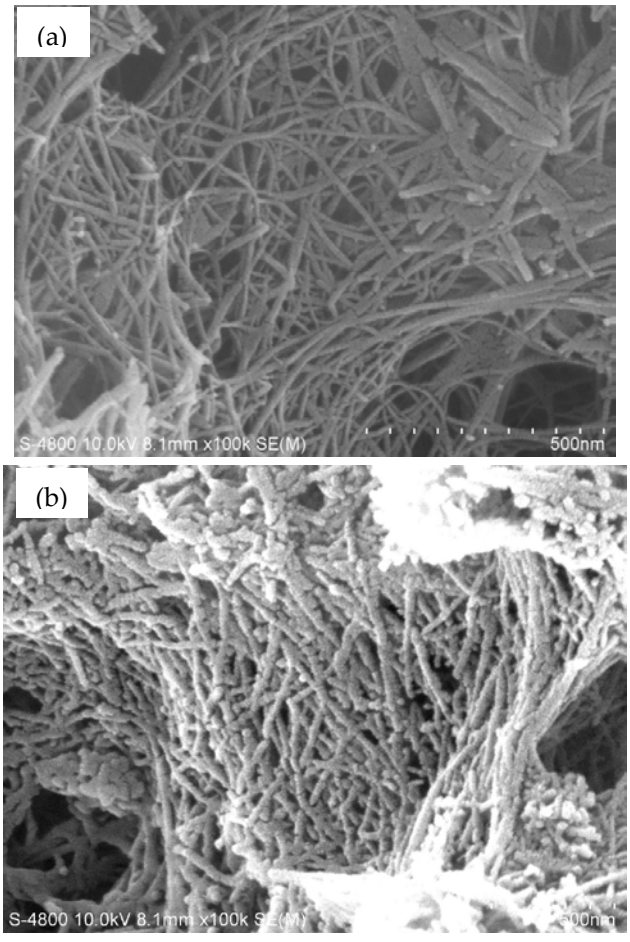

FIG.1. SEM IMAGES OF (a) TIO_2 NANOFIBERS (b) W-DOPED TIO_2 NANOFIBERS

XRD Analysis

Fig. 2a shows the comparison of the XRD pattern of pristine P25, P25 nanofiber and 5 wt% W-doped P25 nanofibers. The result of the diffraction peaks obtained confirms the formation of TiO_2 anatase phase [JCPDS No. 21-1272, space group: I41/amd (1 4 1)]. As shown in Fig. 2a, there are two anatase phase in the pristine P25 with diffraction peak at 25.4° and 48° for (1 0 1) phase and (2 0 0) phase, respectively. The intensity of anatase peaks decreased and the width of XRD diffraction peaks of anatase became wider as it went from pristine to doped TiO_2 nanofiber. The degree of crystallinity decreased as the sample was subjected to further calcination. W peaks were not significant in all the samples. This could be attributed to the low wt% of W and the fact that some of the Ti^{4+} that are on the lattice of TiO_2 nanofiber could be substituted with the $W^{n+}(4<n<6)$, which has similar ion radius (Saepurahman, 2010; Habazaki, 1998). This was clearly elucidated in Fig. 2b where a slight shift towards lower 2θ at the (101) diffraction peak position can be observed as it went from pristine to W doped TiO_2 nanofiber at various concentrations. The peaks have shifted more towards lower 2θ and peak broadening was observed as the concentration increased from 1% wt to 10% wt. As explained earlier, the ionic radius of W^{n+} (4<n<6) (41 pm) smaller than Ti^{4+}(53 pm) (Yang, 2005) is indicative of a decrease in the crystal size.

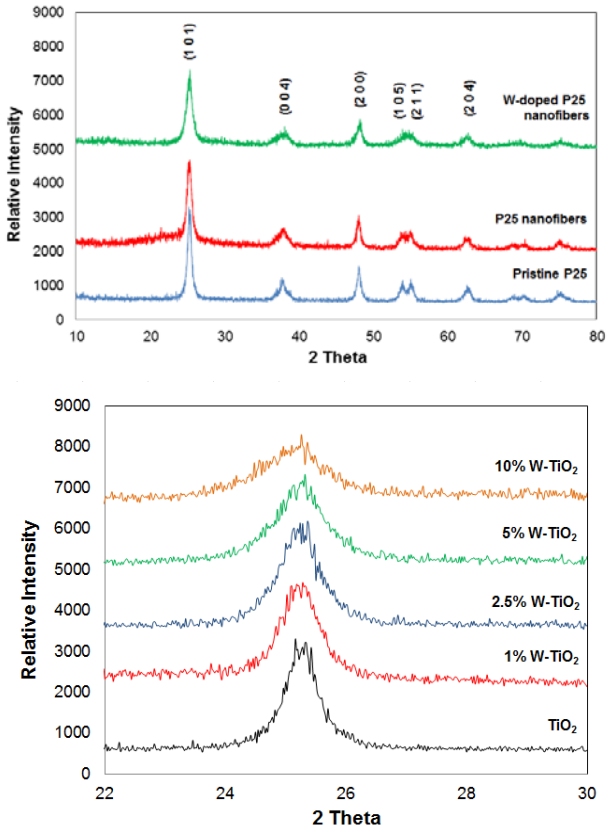

FIG. 2(a) XRD PATTERN OF P25, TIO_2 NANOFIBER AND 5 WT% W-DOPED TIO2 NANOFIBER (b) A ZOOM OF THE (101) DIFFRACTION PEAKS OF TIO_2 NANOFIBER, 1 WT%, 2.5 WT% ,5 WT% AND 10 WT%; W-DOPED TIO_2 NANOFIBER

However, as reported by Yang et.al (2005), a shift in lower 2θ angle generally indicates a lattice volume expansion, which is contrary to the decrease of crystal size. In the present work, no increase of crystal size was observed, thus confirming that the lower angle shift is indicative of mild lattice strain that arises from the possible repulsion between W^{6+} cations, which may occur as interstitial dopants in the bulk of the material. The XRD results here corroborate with the reported work (Yang, 2005).

BET Surface Area and Pore Structure Analysis

Fig. 3 shows the nitrogen adsorption-desorption isotherms and corresponding pore size distribution curves of the W-doped TiO_2 nanofiber. The presence of mesopores (2-50 nm) on the sample was observed with the hysteresis loops of type H3 at relative pressure (P/P_o) of range 0.8-1.0. The presence of macropores (>50 nm) on the samples were also seen with the approaching of hysteresis loops to relative pressure of 1.0.

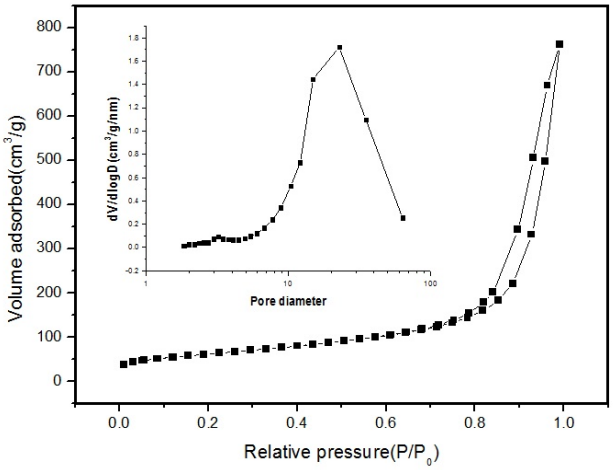

FIG. 3 NITROGEN ABSORPTION TO THE RELATIVE PRESSURE TEST OF W-DOPED TIO_2

TABLE 1 BET SURFACE AREA, PORE VOLUME AND PORE SIZE DISTRIBUTION OF THE W-DOPED TITANIA AT VARIOUS W DOPING CONCENTRATIONS

Samples	Surface area (m^2/g)	pore volume (cm^3/g)	Average Pore Size (nm)
TiO_2	112.4	0.99	35.3
1% W-TiO_2	128.7	1	31.1
2.5%W-TiO_2	157.4	1.14	29
5% W-TiO_2	197.2	1.25	25.4
10% W-TiO_2	220.3	1.18	21.4

Table 1 shows the BET test result of different W doping concentrations obtained from the nitrogen adsorption-desorption isotherm data. BET surface area (S_{BET}) of the W-doped Titania nanofiber increased with the increasing wt% of W. Higher specific surface was attributed to the W-doping which inhibited the growth of TiO_2 nanofiber. The smaller the crystallite sizes of materials were, the higher the specific surface area was. As shown in the Table 1, the pore size distribution of the W-doped Titania nanofiber has also increased as the W doping concentration increased.

Light Absorption Characteristics

Fig. 4 shows the UV-Vis spectra of the photocatalyst samples. The absorption threshold of pristine P25 occurred at ~400 nm and an abrupt increase in absorption before 400 nm can be observed because of the intrinsic band gap energy of TiO_2 (3.2 eV). As the absorption spectra were extended, a red shift can be seen for the W-doped Titania nanofiber as the wt% of W increases; the higher the wt% of W in the composite was, the larger the absorption threshold of the samples was. This was influenced by the doping of W into the Titania nanofiber, which was attributed to the charge transfer transition on Titania nanofiber conduction band (Chen and Mao, 2007). The sample doped with 5% of W and 10% of W showed similar absorption on in the 500-800 nm regions of visible light but the latter showed a higher absorption on the region of ultraviolet region. This is because of the crystal distortion that increases as doping concentration increases. When more W6+partly substitutes Ti^{4+} in the TiO_2 lattice, and the absorption edge of TiO_2 red shifts to a longer wavelength. Although, higher degree of crystal distortion could induce more carriers to be generated under visible light irradiation (Chen and Mao, 2007), which will increase the photocatalytic efficiency but sample doped with 5% of W was found to show higher photocatalytic activity than 10% of W. The drop in photocatalytic efficacy as the doping concentration exceeds 5% is attributed to the increase in the recombination centres produced by W for the photogenerated carriers.

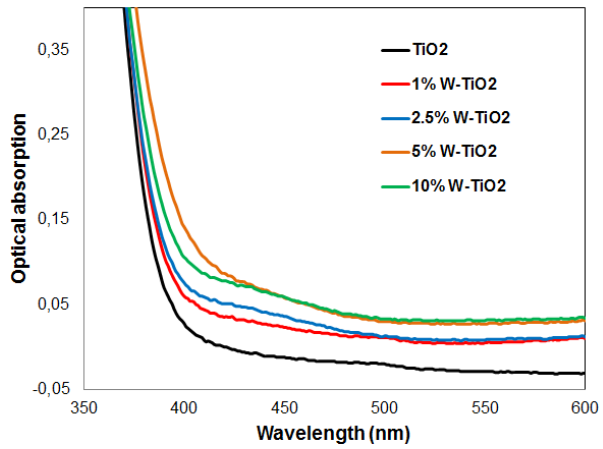

FIG. 4 UV-VIS SPECTRA OF THE W-DOPED TIO_2 NANOFIBER WITH DIFFERENT WT% OF W

Photocatalytic Activity

The hydrogen production rate of W-doped Titania nanofiber in 20% methanol aqueous solution has been reported as an effective hole scavenger to prevent electron hole recombination. In Fig. 5, the hydrogen production rate shows an increasing pattern, as the wt% of W increases from 1% (209.08 $\mu molH_2h^{-1}$) to 5% (790.63 $\mu molH_2h^{-1}$). As the loading of W goes beyond 5%, the hydrogen production of sample materials started decreasing. The excess loading of WO_3 creating recombination site of photocatalysis process has reduced the hydrogen production. The photocatalytic activity of sample was evident from the W-doping as it created means of transfer of photogenerated electrons from TiO_2 to W. The enhancement of absorption intensity in visible light range has induced more photogenerated electrons and holes, giving rise to the photocatalytic activity.

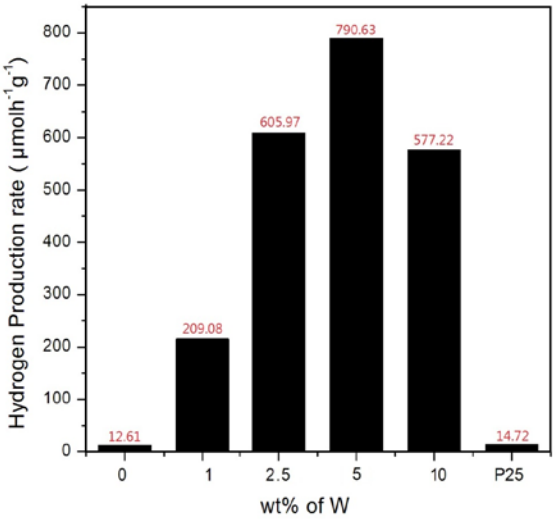

FIG. 5 PHOTOCATALYTIC HYDROGEN PRODUCTION RESULT OF THE W-DOPED TIO_2 NANOFIBER WITH DIFFERENT WT% OF W

Conclusions

A light driven strategy was demonstrated with the preparation of W-doped TiO_2 nanofiber. W-doping into TiO_2 nanofiber has influenced the change of crystallinity, specific surface areas and pore structures. The photocatalytic activities of the samples were greatly enhanced by yielding 60 times higher hydrogen production with the increase of W-doping into TiO_2 nanofiber at an optimal doping level of W, i.e. at 5 wt%. The doping has induced a shift in the absorption light range with the narrowing of the bandgap energy. The increase in the photocatalytic activity of the W-doped TiO_2 has indicated the improvement of the transportation of charge transfer on the Titania nanofiber conduction band and reduced the electron-hole recombination rate. However, the further increase of W-doping into TiO_2 nanofiber has led to reduction of photocatalytic activity.

ACKNOWLEDGMENT

We gratefully acknowledge the support from State key laboratory of advanced technology for Materials synthesis and processing (SKLWUT), Wuhan University of Technology (WHUT) for SEM, XRD, and Gas-chromatograph analysis.

REFERENCES

Arai T., Senda S., Sato Y., Takahashi H., Shinoda K., Jeyadevan B. and Tohji K., Cu-Doped ZnS Hollow Particle with High Activity for Hydrogen Generation from Alkaline Sulfide Solution under Visible Light Chem. Mater., 20 (2008): 1997-2000.

Chen X., and Mao S. S., Titanium dioxide nanomaterials: synthesis, properties, modifications, and applications, Chem. Rev., 107 (2007): 2891–2959.

Colon G., Maicu M., Hidalgo M., Navio J. , Cu-doped TiO systems with improved photocatalytic activity, Appl Catal. B-Environ, 67 (2006): 41-51.

Couselo N., Garcia Einschlag F. , Candal R., Jobbagy M. , Tungsten-Doped TiO_2 vs Pure TiO_2 Photocatalysts: Effects on Photobleaching Kinetics and Mechanism J. Phys. Chem. C, 112 (2008): 1094-1100.

Dholam R., Patel N., Adami M., Miotello A. , Hydrogen production by photocatalytic water-splitting using Cr- or Fe-doped TiO_2 composite thin films photocatalyst, Int. J. of Hydrog. Energy, 34 (2009): 5337-5346.

Fujishima A. and Honda K. , Photocatalyst materials for water splitting, Nature, 238 (1972): 37-38.

Fujishima A., Rao T. N., and Tryk D. A., Titanium dioxide photocatalysis, J Photochem Photobiol C Photochem Rev, 1 (2000)

Fujishima A., Zhang X., Tryk D. A. , TiO_2 photocatalysis and related surface phenomena, Surface Science Reports, 63 (2008): 515-582.

Habazaki H., Takahiro K., Yamaguchi S., Shimizu K., Skeldon P., Thompson G.E., Wood G. C. , Influence of tungsten species on the structure of anodic titania , Philosophical Magazine A, 78 (1998): 171-188.

Hashimoto K.,. Irie H and Fujishima A., TiO_2 Photocatalysis:

A Historical Overview and Future Prospects Jpn. J. Appl. Phys., 44, 12 (2005):8269–8285.

Jung K. Y. and Park S. B. , Enhanced photoactivity of silica-embedded titania particles prepared bysol–gel process for the decomposition of trichloroethylene Appl Catal. B-Environ, 25 (1999): 249-256.

Kanade K.G., Kale B.B., Baeg J. O, Lee S. M., Lee C. W., Moon S. J., Chang H. , Self-assembled aligned Cu doped ZnO nanoparticles for photocatalytic hydrogen production under visible light irradiation, Materials Chemistry and Physics, 102 (2007): 98-104.

Kaneko M. and Okura I. ,Photocatalysis: science and technology: Springer-Verlag (2002).

Kasuga T., Hiramatsu M., Hoson A., Sekino T., and Niihara K., Formation of Titanium Oxide Nanotube Langmuir, 14 (1998): 3160-3163.

Khan M. A., Woo S. I., Yang O.B, Hydrothermally stabilized Fe(III) doped titania active under visible light for water splitting reaction Int. J. of Hydrog. Energy, 33 (2008): 5345-5351.

Kudo A. , Photocatalyst Materials for Water Splitting, Catalysis Surveys from Asia, 7 (2003): 31-38.

Lorret O., Francova D., Waldner G., Stelzer N. , W-doped titania nanoparticles for UV and visible-light photocatalytic reactions, Appl Catal. B-Environ:91 (2009): 39-46.

Marci G., Palmisano L., Sclafani, Venezia A.M. , Campostrini R., Carturan G., Martin C., Rives V. , Solana G., Influence of tungsten oxide on structural and surface properties of sol–gel prepared TiO_2 employed for 4-nitrophenol photodegradation , J Chem Soc Faraday Trans 92 (1996): 819–82.

Putta T., Lu M. C., Anotai J. , Photocatalytic activity of tungsten-doped TiO_2 with hydrothermal treatment under blue light irradiation, J. of Environ Management ,92 (2011): 2272 -2276.

Saepurahman, Abdullah M. A., Chong F. K., Preparation and characterization of tungsten-loaded titanium dioxide photocatalyst for enhanced dye degradation J. Hazard M., 176 (2010): 451-458.

Shen Y., Xiong T., Li T., Yang K. , Tungsten and nitrogen co-doped TiO_2 nano-powders with strong visible light response, Appl Catal. B-Environ, 83 (2005): 177-185.

Wu W., Hu X., Xie T., Li G., Zhang L., Phase Structure of W-Doped Nano-TiO_2 Produced by Sol-Gel Method, China Particuology 3 (2005): 233-236.

Yang H. M., Shi R. R., Zhang K., Hu Y. H., Tang A. D. and Li X.W. , Synthesis of WO_3/TiO_2 nanocomposites via sol–gel method Alloy Compd 398 (2005): 200–202.

Zhou M., Yu J., Cheng B., Yu H. , Preparation and photocatalytic activity of Fe-doped mesoporous titanium dioxide nanocrystalline photocatalysts, Materials Chemistry and Physics, 93 (2005): 159-163.

Zhou M., Yu J., Cheng B. , Effects of Fe-doping on the photocatalytic activity of mesoporous TiO_2 powders prepared by an ultrasonic method, J. Hazard M., 137 (2006): 1838-1847.